J. Cent. South Univ. (2020) 27: 10−17
DOI: https://doi.org/10.1007/s11771-020-4273-6

Springer

Microstructure and mechanical properties of three kinds of titanium alloys by SPS

YANG Xin(杨鑫)[1], SHI Ming-jun(时明军)[2], LIU Shi-feng(刘世锋)[2], LI An(李安)[2]

1. College of Materials Science and Engineering, Xi'an University of Technology, Xi'an 710048, China;
2. School of Metallurgical and Engineering, Xi'an University of Architecture & Technology, Xi'an 710055, China

Abstract: High-density titanium alloys with different grains were prepared by spark plasma sintering (SPS) at 900 °C and 15 MPa using spherical powder generated by the plasma rotating electrode process (PREP) and nonspherical powders generated by hydrogenation-dehydrogenation (HDH) and molten salt electrolysis (MSE) as raw materials. Studies have shown that the PREP sample is a dense lamellar α structure and that the sample is clean. The microstructure of the HDH sample is composed of equiaxed α and lamellar α structures, and there are many flaws on the surface of the sample. The MSE samples are composed of α lamellar and coarse equiaxed crystals. The integral grain size is bulky, there are many irregular pores in the samples, and the samples are not clean. Of the three samples, the HDH sample has the largest compressive strength (526.85 MPa) and hardness (HV 293.1) but poor plasticity (compression strain is 26.61%); the compressive strengths of the PREP and MSE samples are 268.47 and 251.23 MPa, the compressive strains are 45.08% and 17.44%, and the microhardness values are HV138.6 and HV203.4, respectively.

Key words: titanium powders; spark plasma sintering; microstructure; mechanical properties

Cite this article as: YANG Xin, SHI Ming-jun, LIU Shi-feng, LI An. Microstructure and mechanical properties of three kinds of titanium alloys by SPS [J]. Journal of Central South University, 2020, 27(1): 10−17. DOI: https://doi.org/10.1007/s11771-020-4273-6.

1 Introduction

Pure titanium has one of the highest hydrogen absorption densities and has been used as a hydrogen storage material or tritium storage target [1, 2]. At present, titanium is used as a storage element for the reaction energy of tritium-deuterium thermonuclear fusion. However, some deficiencies still exist, for example, the grain size is coarse, and the grain boundary is low. The helium produced by tritium decay will accumulate at the grain boundary, which will lead to material failure when the helium concentration exceeds the critical threshold [3−5]. Developing new tritium solid helium storage materials is of great strategic significance and economic value. An effective way to improve the properties of these storage materials is by refining the grains and increasing the internal interface of the materials. SPS technology combines hot pressing, electric resistance heating and plasma activation, and the spark discharge instantly

Foundation item: Projects(51671152, 51304153, 51504191, 51874225) supported by the National Natural Science Foundation of China; Project(14JK512) supported by Natural Science Foundation of Shaanxi Educational Committee, China; Project(18JC019) supported by Shaanxi Provincial Department of Education Industrialization Project, China; Project(14JK1512) supported by Shaanxi Provincial Department of Education Natural Science Special Project, China
Received date: 2018-10-28; **Accepted date:** 2019-07-02
Corresponding author: LIU Shi-feng, PhD, Professor; Tel: +86-29-82202933; E-mail: liushifeng66@126.com; ORCID: 0000-0003-4369-5730

produces plasma, which evaporates the oxide layer on the powder surface to purify and activate while simultaneously reducing the atom diffusion free energy and realizing rapid prototyping of the fine crystal material [6−12]. PANG et al [13] found that the helium storage capacity of thin titanium materials is much higher than that of coarse crystalline material. The He/Ti atomic ratio of nanocrystalline titanium films with grain sizes of 10−20 nm can reach 35% to 48%.

Hydrogenation-dehydrogenation (HDH), molten salt electrolysis (MSE) and the plasma rotating electron processing (PREP) are three important methods for preparing titanium powder [14]. HDH is the most mature and widely used titanium powder production method at present. It usually requires low-performance and inexpensive raw materials, but the powder grain size distribution is wide, and the fluidity is poor. The oxygen and nitrogen contents are relatively high [15]. The preparation of titanium powder by MSE shows unparalleled value and advantages in reducing the cost and shortening the production cycle. In recent years, great progress has been made in the preparation of high-purity and low-cost titanium powder by using MSE [16]. The PREP method is a common method for the preparation of high-quality spherical titanium powder based on the centrifugal force of droplets rotating at high speed and the effect of surface tension on the formation of spherical particles in an inert atmosphere [17]. In order to study the effect of powder prepared by different processes on the properties of the sample, three different kinds of powders were used as raw materials to prepare high-density titanium alloys with different grains size at a sintering temperature of 900 °C and a sintering pressure of 15 MPa by spark plasma sintering (SPS). The microstructures and mechanical properties of the samples were studied.

2 Experimental

Different titanium powders generated by PREP, HDH and MSE were used as raw materials, and a graphite mold and HP D25/3-type spark plasma sintering furnace were used in the experiment. The sintering temperature was 900 °C, and the sintering pressure was 15 MPa. The heating rate was 150 °C/min from 0 to 700 °C, 100 °C/min from 700 °C to 800 °C, 50 °C/min from 800 °C to 850 °C, and 25 °C/min from 850 to 900 °C. After maintaining constant pressure for 5 min, a *d*40 mm sample was obtained as the furnace cooled to room temperature. The density of the samples was determined by the Archimedes method. The microstructure of the sample was measured by an OLMPUS-PMG3 optical microscope. The pore morphology of the powder and sintered sample was observed by a JSM-6700F scanning electron microscope (SEM), and the phase structure of the powder and sample was measured by a D8 ADVANCE A25 XRD using Cu Kα irradiation at 40 kV from 30° to 90°, and the scanning step size was 0.02°. The compression properties of the samples were tested by an INSTRON-3369 test machine; the compressed sample sizes were *d* 6 mm×9 mm and the loading rate was 0.5 mm/min.

3 Results and discussion

3.1 Phase analysis of titanium powder made by different process

Figure 1 shows the SEM image of the original powder and the XRD diffraction pattern. It can be seen that the whole surface of the PREP powder is smooth, the shape is regular and spherical, and a “satellite ball” or flake powder is not observed. This is related to the preparation process of the PREP powder. Molten metal droplets were emitted from the bar under centrifugal force, and then a powder with a high degree of sphericity was formed as a result of surface tension. The number of particles with diameters less than 100 μm increased, and no obvious difference in the size of the large particle powder was observed. There is no significant difference between the size of fine particles in the powder and the maximum particle size of less than 200 μm. The shape of the HDH powder is irregular, and the angle is high. For the obvious mechanical crushing characteristics, the large powder particles form a more compact agglomeration, and the surface is rough. The morphology and particle size of the MSE powder differ from those of the HDH powder, but the MSE sample mainly exists in powder shape and a dense particle state. The fine powder particle size is relatively uniform, but the surface is rough and aggregates into a spongy shape, and the powder has large pores. Fine dendritic particles can be observed on some of the rough

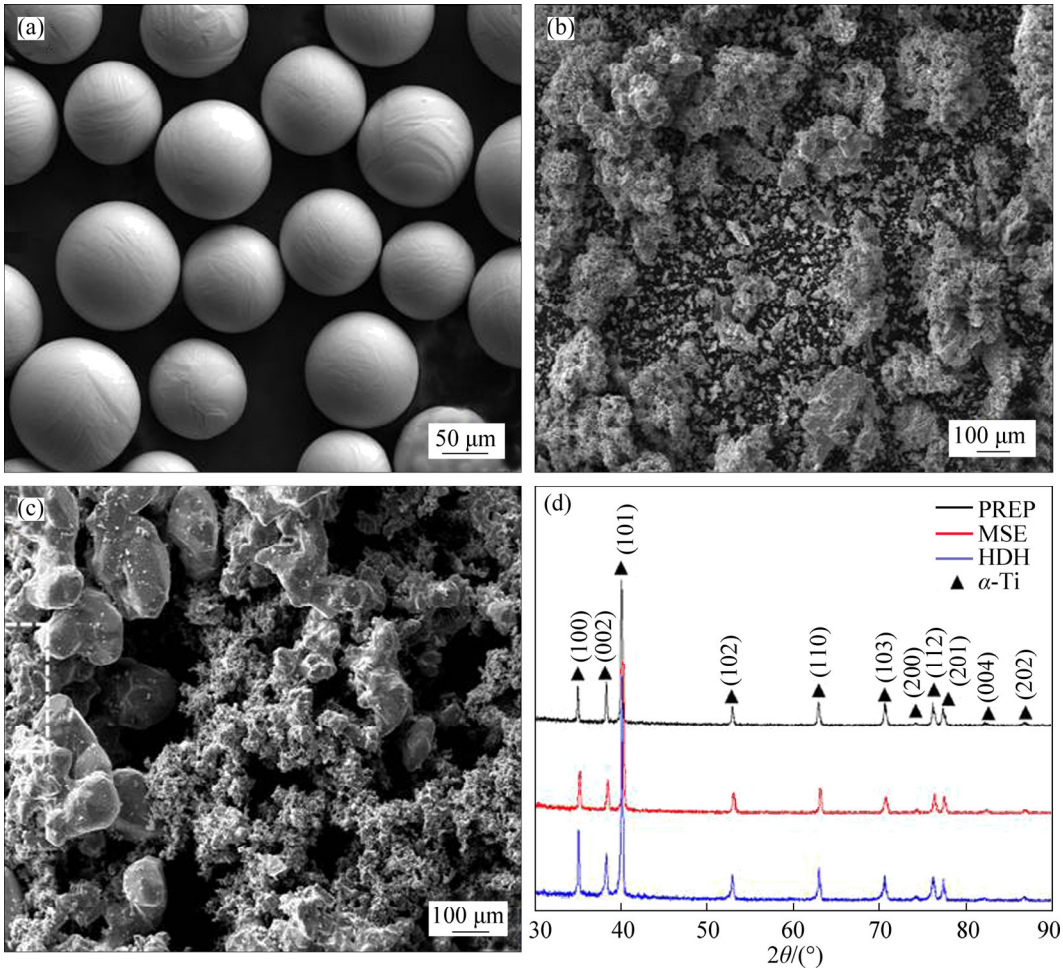

Figure 1 SEM images of original powder and XRD diffraction patterns: (a) PREP; (b) HDH; (c) MSE; (d) XRD

powder surfaces, as shown by the rectangular wire frame in the Figure 1(c), and the surface of the large powder particles is more compact and smoother. The results show that the particle size of MSE titanium powder is related to the concentration of titanium ions in the molten salt system. When the concentration of titanium ions is low, the crystal nucleus is difficult to grow, eventually forming smaller titanium powder particles. When the concentration of titanium ions is high enough, the crystal grain nucleates and grows. Finally, more compact large titanium powder particles were obtained.

Compared with the results of the PREP spherical titanium powder, the shapes of the HDH and MSE powders are irregular, the HDH and MSE powders are looser, and the apparent density is higher than that of the PREP powder. It is easy for the powders to absorb air moisture, oxygen, nitrogen and other impurities, thus reducing the compression and sintering properties of the powder. However, the higher oxygen content easily forms an oxide film on the surface of the sample, which is not conducive to the diffusion and absorption of tritium helium in the tritium solid helium storage element.

The XRD patterns of the three kinds of powders show that the diffraction peaks on the crystal planes of HDH and MSE are strong and sharp. At the same time, no abnormal diffraction peaks have been observed, which indicates that the crystallinity of the original HDH and MSE powders is high. In addition, the diffraction peaks of the HDH powder were obviously narrower and sharper than those of the MSE sample, and the diffraction peak intensity was enhanced. The results show that the crystallization degree of the HDH powder is higher and the grain size is more uniform than those of the MSE sample. Compared with the XRD patterns of PREP powders, the diffraction peak intensity is decreased, and the diffraction peak type of the PREP powder is narrower.

3.2 Microstructural analysis of samples prepared by different processes

Figure 2 shows the microstructure of SPS-sintered samples. Figure 2(a) shows that the microstructure of the HDH sample is roughly composed of two forms after sintering by SPS: the equiaxed α structure and a small amount of coarse α lamellar structure (B) in Figure 2(a). The equiaxed α structure is composed of double-scale equiaxed crystals, that is, the fine equiaxed α structure with a grain size less than 1 μm and the coarse equiaxed α structure (5−15 μm) with a small quantity of grains larger than 20 μm; the α-lamellae are short and thick and interlaced into a net basket structure. There are only a few holes in the sample and the relative density of the sample is 98.68%. Figure 2(b) is a high-magnification metallographic structure of a sample prepared by SPS using HDH powder as a raw material, and the whole structure is composed of lamellar α and equiaxed α (shown as A in Figure 2(b)), and the surface of the sample exhibits partial microcrack defects. The microstructures of the MSE samples are composed of equiaxed α-structure (A) in Figure 2(c) and coarse lamellar α-tissue (shown in Figure 2(c) B). Compared with the HDH samples, the α grains in the samples are larger as a whole, and most of the equiaxed α crystal sizes are approximately 5−20 μm. MSE grain sizes greater than 20 μm are larger than those of the HDH sample, and some grains reach 30 μm. In the microstructural images, α lamellar layer is fine and long, the thickness of α lamellar layer is 20−50 μm, and the length is 50−150 μm. There are many holes in the MSE sample, and the larger pores can be observed; most of them are distributed along the boundary of the original particles. The relative density of the sample is 95.74%. In addition, there are many small pores scattered in the equiaxed crystal region of the sample, and the pore shape is relatively smooth and subject to spheroidization. Figure 2(d) shows a metallographic structure of the PREP sample. The

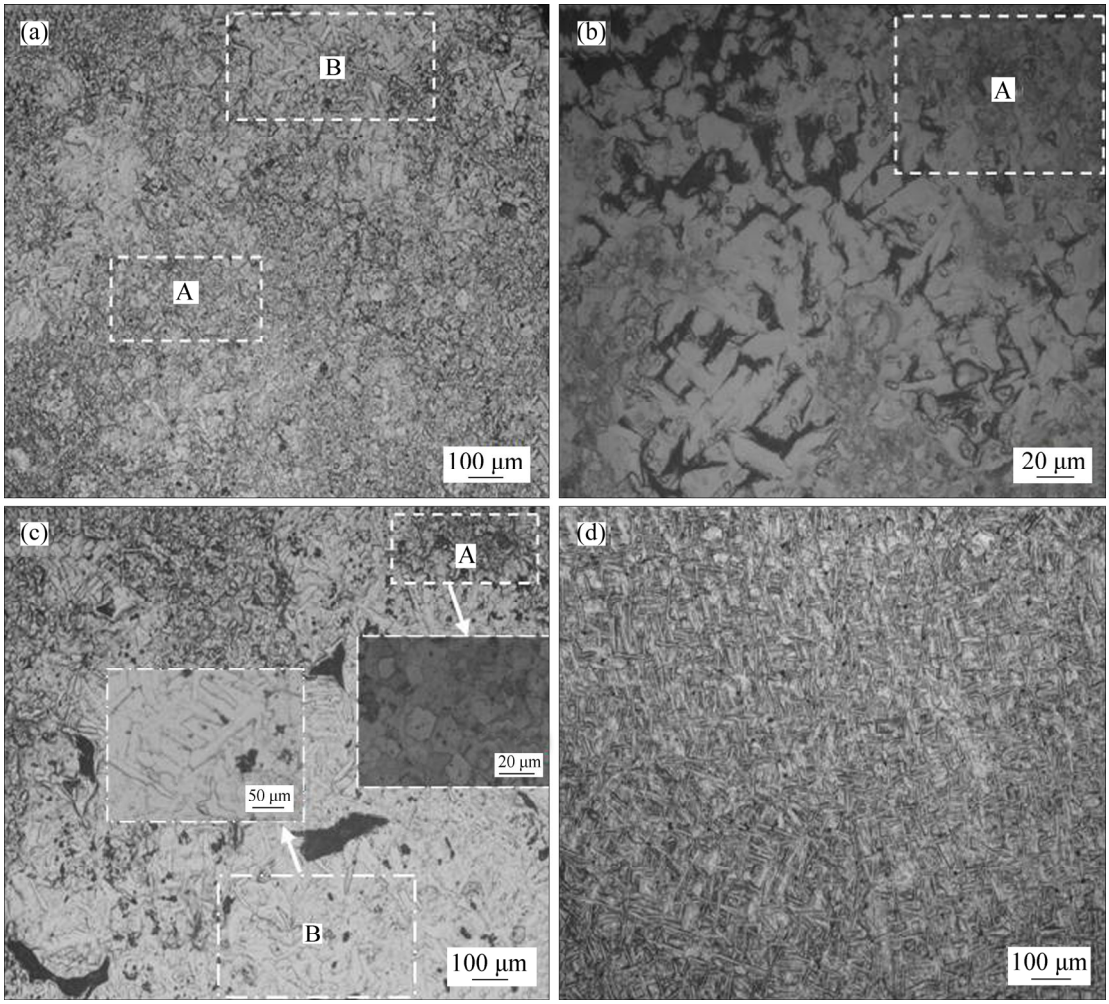

Figure 2 Microstructure of different SPS samples: (a, b) HDH; (c) MSE; (d) PREP

PREP samples showed dense baskets with a thickness of 2−10 μm and a length of 20−100 μm. Only a small number of small spherical pores were observed between the α-layers. The relative density of the sample is 98.42%.

Figure 3 shows SEM images of the HDH and MSE samples. It can be seen that the whole HDH sample is compact, and there are no coarse pores in the sample; only a few fine pores can be observed, which indicates that the HDH powder is fully sintered after mechanical crushing. Partial plastic deformation of the powder and a small number of dislocations occur, while during sintering, dislocations are easily diffused. In addition, a large number of thin microcracks were observed in the HDH samples, and the crack size was 50−200 μm. Because of the complex and irregular shape of HDH powder, the "arch bridge" effect occurred easily, which resulted in uneven pressure transfer from the surface to the center of the sheet and ultimately formed a crack. At the same time, during SPS sintering, there exists a certain temperature gradient between the core and the edge of the sample, and the cooling rate between the core and the edge is inconsistent during the cooling process of the sample. Cracks are produced by residual stress release during sample cooling. The matrix of the MSE sample is compact but irregular. The polygonal pores are coarse, and there are many dark impurity oxides in the pores. Under high magnification, the pore size is 5−10 μm, and the fine pores are nearly circular or elliptical compared with the coarse pores. The acuity angle of the pores is obvious, and the passivation surface is relatively smooth.

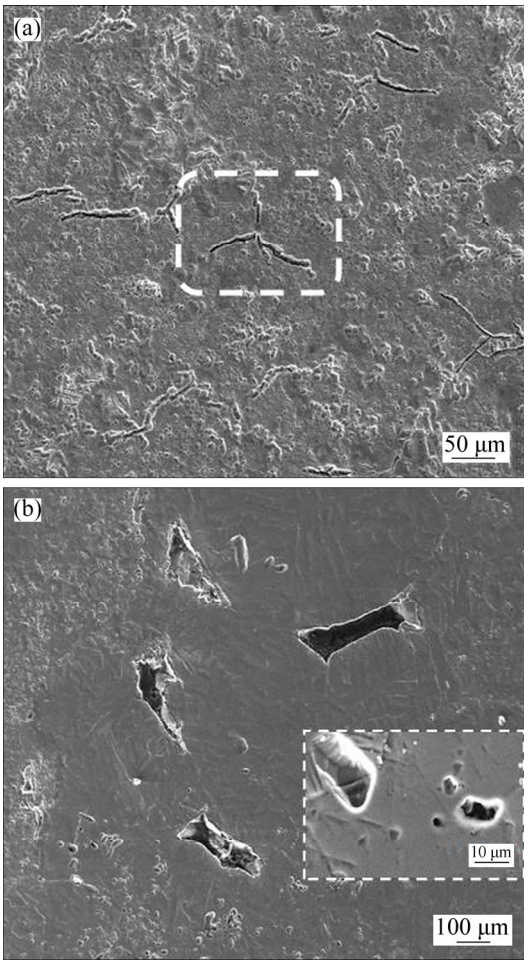

Figure 3 SEM images of HDH and MS samples: (a) HDH; (b) MSE

3.3 Compression properties and microhardness analysis of PREP, HDH and MSE samples

Figure 4 shows the compressive stress−strain curves of different specimens at room temperature. The yield strength of the PREP sample is 90.25 MPa. With increasing stress, the relationship between stress and strain is approximately a first-order function. The compressive strength is lower than 268.47 MPa, but the compressive strain is up to 45.08%, and the plasticity is good. When the HDH sample is compressed, the elastic deformation of the sample is approximately 5%, and the yield strength is approximately 236.36 MPa compared with the PREP sample. With increasing pressure, the stress−strain is similar to that of the PREP sample, and the linear relationship is similar to that of the PREP sample. When the stress reaches 526.85 MPa, the crack in the sample propagates and eventually leads to fracture of the sample. The high tensile strength of HDH samples may be explained

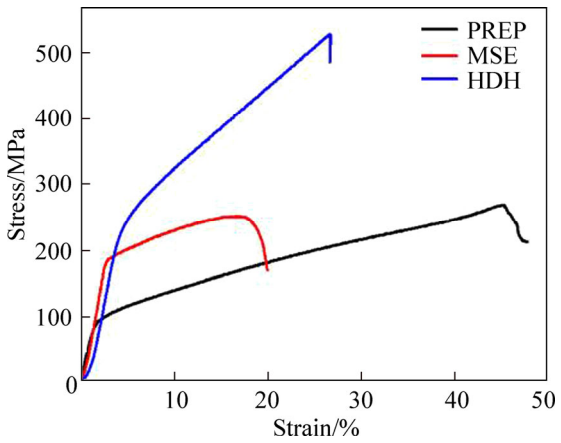

Figure 4 Stress−strain curves of different sintered samples

by the influence of a large number of equiaxed α and lamellar α staggered, the crack is easily bifurcated to form a secondary crack, so the propagation path of the crack in the lamellar structure is more tortuous, resulting in an increase in the total length of the crack and requiring more energy to be consumed. Compared with those of the HDH samples, the pores in the MSE samples deformed rapidly with an increase in pressure at the plastic deformation stage until the final collapse and densification. The density was 95.74%, the yield strength was 183.03 MPa, the compressive strength was 251.23 MPa, and the strain was only 17.44% because of the existence of the pores in the samples. Compared with PREP samples, the compressive strain of the HDH and MSE samples decreased significantly and showed poor plasticity. The corresponding elastic moduli were 6.06 GPa and 7.07 GPa, respectively, which are slightly higher than that of the PREP samples (5.32 GPa).

According to the Vickers hardness diagram of the samples (Figure 5), the microhardness of the MSE and HDH amples significantly increased to HV 203.4 and HV 293.1, respectively, compared with that of the PREP sample (HV 138.6). Figure 2(a) shows that the samples are compact and have more fine equiaxed α in their microstructure. According to the Hall-Petch formula, the finer the grain in the sample is, the higher the strength of the material is and the higher the hardness of the HDH sample is. There are still fine equiaxed α structures in the same sample, but the quantity is reduced greatly, the density of the sample is slightly lower than that of the HDH sample, and the hardness is slightly lower. However, the microhardness of the two kinds of SPS powder samples is higher than that of the PREP sample. Table 1 lists the microstructure, relative density, microhardness and compression properties of samples prepared from three powders.

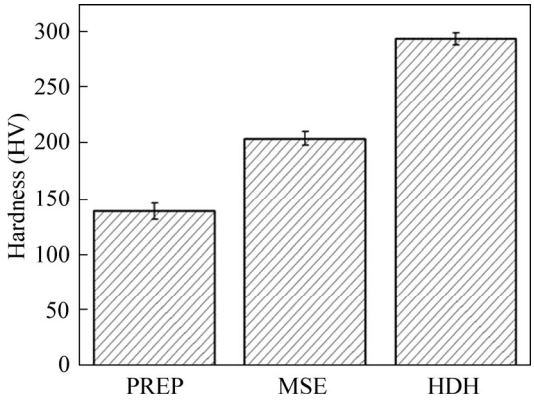

Figure 5 Vickers hardness of different sintered samples

4 Conclusions

Titanium alloys based on PREP, HDH and MSE were prepared by SPS. Research shows that the cost of HDH powder is lower, but the comprehensive mechanical properties of sintered samples are better, which has great application prospects as raw materials for titanium alloys. However, how to reduce the formation of TiH and reduce the surface defects in the process of preparing titanium alloy from HDH powder needs further investigation.

1) The sphericity of PREP powders is high, and the powder surface is smooth. The shape of the HDH powder is irregular. The particle size of the MSE powder is different, with fine powder particles gathered into a sponge-like structure; the powder is fine dendrite, and the surface of the powder is relatively smooth. The HDH and MSE powders are loose, and the pores are looser; the XRD analysis shows that three kinds of powder are formed. These samples showed only a single phase, with no impurity or alloy phase diffraction peak.

2) The PREP sample is a compact lamellar α tissue that is highly clean, and the microstructure of the HDH sample is composed of ISO axis α and lamellar α tissues; there are few small pores in the

Table 1 Microstructure, relative density, microhardness and compression properties of samples prepared from three powders

Sample	Microstructure	Relative density/%	Hardness (HV)	Elastic modulus/GPa	Compressive strength/MPa	Compressive strain/%
PREP	Lamellar α	98.42±0.43	138.6±6.82	5.32±0.24	268.47±4.63	45.08±0.76
HDH	Equiaxed α and lamellar α	98.68±0.32	293.1±7.24	6.06±0.11	526.85±8.90	26.61±0.44
MSE	Lamellar α and coarse equiaxed α	95.74±0.36	203.4±6.40	7.07±0.26	251.23±6.22	17.44±0.97

sample, and there are many cracks on the sample surface. The MES samples are composed of coarse equiaxed grains and α lamellas, but the grain is relatively coarse, and irregular pores are contained in the samples. There are many impurities and oxides, and the cleanliness is poor.

3) The compressive strengths of PREP, HDH and MSE samples were 268.47, 526.85 and 251.23 MPa, respectively, and the compressive strains were 45.08%, 26.61% and 17.44%, respectively. The microhardnesses were HV 138.6, HV 203.4 and HV 293.1, respectively.

References

[1] UESUGI T, MYAMAE S, TAKIGAWA Y, HIGASHI K. Alloying effects of transition metals on beta phase stability of Ti alloys from first-principles calculations [C]// Proceedings of the 13th World Conference on Titanium. John Wiley & Sons, Inc. 2016. DOI: 10.1002/9781119296126.ch321.

[2] WANG Hai-feng, PENG Shu-ming, ZHOU Xiao-song, CHENG Gui-jun, WANG Wei-du, LONG Xing-gui, YANG Ben-fu. Primarily study on thermodesorption from titanium tritide films [J]. Atomic Energy Science and Technology, 2008, 42(1): 49−52. http: //www. cnki. com.cn/Article/CJFDTotal-YZJS200801010. Htm. (in Chinese)

[3] BUSQUÉ, RAQUEL, TORRES R, GRAU J, RODA V, HUSAR A. Mathematical modeling, numerical simulation and experimental comparison of the desorption process in a metal hydride hydrogen storage system [J]. International Journal of Hydrogen Energy, 2018, 43(35): 16929−16940. DOI: 10. 1016/j. ijhydene. 2017.12.172.

[4] SHEN Hua-hai, PENG Shu-ming, LONG Xing-gui, XIANG Xia, ZHOU Xiao-song, YANG Li, ZU Xiao-tao. Microstructure changes of erbium and erbium deuteride films induced by helium implantation [J]. Materials Letters, 2012, 80(8): 17−19. DOI: 10.1016/j.matlet.2012.04.084.

[5] FLANAGAN T B, WANG D, LUO S. Thermodynamics of hydrogen absorption (desorption) in unoxidized and internally oxidized Pd–Ti alloys [J]. Journal of Alloys and Compounds, 2017, 701(4): 981−992. DOI: 10.1016/j.jallcom. 2016. 12. 290.

[6] ZAREBSKI K, PUTYRA P. Iron powder-based graded products sintered by conventional method and by SPS [J]. Advanced Powder Technology, 2015, 26(2): 401−408. DOI: 10.1016/j.apt.2014.11.010.

[7] PARASKEVAS D, VANMEENSEL K, VLEUGELS J, DEWULF W, DUFLOU J R. The use of spark plasma sintering to fabricate a two-phase material from blended aluminum alloy scrap and gas atomized powder [J]. Procedia CIRP, 2015, 26: 455−460. DOI: 10.1016/j.procir.2014.07.074.

[8] ZHAO Kun, LIU Yong, HUANG Lan, LIU Bin, HE Yue-hui. Diffusion bonding of Ti-45Al-7Nb-0.3W alloy by spark plasma sintering [J]. Journal of Materials Processing Technology, 2016, 230(4): 272−279. DOI: 10.1016/j.jmatprotec.2015.11.030.

[9] LI An, LIU Shi-feng, WANG Bo-jian, ZHANG Zhao-hui, LIU Quan-ming. Developmental states of porous metal materials prepared by spark plasma sintering [J]. Powder Metallurgy Technology, 2017, 35(5): 378−383. DOI: 10.19591/j.cnki.cn11-1974/tf. 2017. 05. 010.

[10] LIU Li-meng, HOU Zhao-ping, ZHANG Bao-you, YE Feng, ZHANG Zhi-guo, ZHOU Yu. A new heating route of spark plasma sintering and its effect on alumina ceramic densification [J]. Materials Science & Engineering A, 2013, 559(3): 462−466. DOI: 10.1016/j.msea.2012.08.126.

[11] MONNIER J, CHAMPION Y, PERRIÈRE L, VILLEROY B, GODART C. Spark plasma sintering and hydrogen pre-annealing of copper nanopowder [J]. Materials Science & Engineering A, 2015, 621(5): 61−67. DOI: 10.1016/j.msea.2014. 10. 040.

[12] MARDER R, ESTOURNÈS C, CHEVALLIER G, CHAIM R. Plasma in spark plasma sintering of ceramic particle compacts [J]. Scripta Materialia, 2014, 82(7): 57−60. DOI: 10.1016/j.scriptamat. 2014. 03. 023.

[13] PANG Hong-chao, LUO Shu-zhong, LONG Xing-gui, AN Zhu, LIU Ning, DUAN Yan-min, WU Xing-chun, YANG Ben-fu, WANG Pei- lu, ZHENG Si-xiao. Effects of substrate temperature on helium content and microstructure of nunnery stalling titanium films [J]. Chinese Physics Letters, 2006, 23(12): 3238−3241. DOI: 10.1088/0256-307X/23/12/032.

[14] HUO Dong-xing, LIANG Jing-long, LI Hui, XIE Shan-shan. Research progress on preparation of titanium metal [J]. Foundry Technology, 2017, 38(1): 4−7. DOI: 10.16410/j.issn1000-8365. 2017. 01. 002.

[15] OH J M, ROH K M, LEE B K,SUH C Y, KIM W, KWON H, LIM J W. Preparation of low oxygen content alloy powder from Ti binary alloy scrap by hydrogenation–dehydrogenation and deoxidation process [J]. Journal of Alloys & Compounds, 2014, 593(4): 61−66. DOI: 10.1016/j.jallcom. 2014. 01. 033.

[16] LIU Song-li. A study of preparation of titanium metal by the electrochemical reduction of titanium dioxide in molten salt [J]. Procedia Earth & Planetary Science, 2011, 2(1): 1−6. DOI: 10.1016/j.proeps. 2011. 09. 001.

[17] SHEN Lei, CHEN Gang, ZHAO Shao-yang, YIN Jing-ou, TAN Pin, LI Zeng-feng, TANG Hui-ping, ZHOU Quan. Properties and microstructures of spherical NiTi powders prepared by plasma rotating electrode process [J]. Materials Science & Engineering of Powder Metallurgy, 2017, 22(4): 539−545. http://www.en.cnki.com.cn/Article_en/CJFDTotal-FMGC201704013.htm.

(Edited by HE Yun-bin)

中文导读

三种钛粉末的 SPS 显微组织及力学性能

摘要：以旋转电极(PREP)球形粉末和氢化脱氢(HDH)及熔盐电解(MSE)非球形粉末为原料，采用放电等离子烧结技术在 900 ℃ 和 15 MPa 下制备不同晶粒高致密钛合金。研究表明，PREP 样品为致密的片层 α 组织，样品干洁度较高；HDH 样品显微组织由等轴 α 和片层 α 组织组成，样品表面有较多的裂纹存在；MES 样品由 α 片层和粗大等轴晶组成，晶粒整体较为粗大，样品中存在较多不规则孔隙，干洁度较差。HDH 样品压缩强度最大(526.85 MPa)，硬度最高(HV 293.1)，但塑性较差(压缩应变为 26.61%)；PREP 及 MSE 样品压缩强度分别为 268.47 MPa 和 251.23 MPa，压缩应变分别为 45.08%和 17.44%，显微硬度分别为 HV 138.6、HV 203.4。

关键词：钛粉；放电等离子烧结；显微组织；力学性能